Journal of Statistical Physics, Vol. 68, Nos. 3/4, 1992

Lattice Boltzmann Computational Fluid Dynamics in Three Dimensions

Shiyi Chen,[1,2] Zheng Wang,[1] Xiaowen Shan,[1,3] and Gary D. Doolen[1]

The recent development of the lattice gas method and its extension to the lattice Boltzmann method have provided new computational schemes for fluid dynamics. Both methods are fully paralleled and can easily model many different physical problems, including flows with complicated boundary conditions. In this paper, basic principles of a lattice Boltzmann computational method are described and applied to several three-dimensional benchmark problems. In most previous lattice gas and lattice Boltzmann methods, a face-centered-hypercubic lattice in four-dimensional space was used to obtain an isotropic stress tensor. To conserve computer memory, we develop a model which requires 14 moving directions instead of the usual 24 directions. Lattice Boltzmann models, describing two-phase fluid flows and magnetohydrodynamics, can be developed based on this simpler 14-directional lattice. Comparisons between three-dimensional spectral code results and results using our method are given for simple periodic geometries. An important property of the lattice Boltzmann method is that simulations for flow in simple and complex geometries have the same speed and efficiency, while all other methods, including the spectral method, are unable to model complicated geometries efficiently.

KEY WORDS: Lattice gas; lattice Boltzmann; three-dimensional flows; Turbulence.

1. INTRODUCTION

Lattice gas automata (LGA)[1] and the lattice Boltzmann equation (LBE)[2,3] have been actively considered as alternative numerical methods

[1] CNLS and Theoretical Division, Los Alamos National Laboratory, Los Alamos, New Mexico 87545.
[2] Bartol Research Institute, University of Delaware, Newark, Delaware 19716.
[3] Department of Physics and Astronomy, Dartmouth College, Hanover, New Hampshire 03755.

0022-4715/92/0800-0379$06.50/0

for solving the Navier–Stokes equations for several years. These numerical methods provide new parallel computational algorithms which can be easily programmed on modern parallel computers, including the Connection Machine-2. Both the lattice gas and the lattice Boltzmann method can simulate fluid flows with complicated geometry and complex physics, such as two-phase fluid flows,[4–6] flows through porous media,[7,8] and magnetohydrodynamics.[9,10]

The lattice Boltzmann equation is an extension of lattice gas automata which uses real numbers instead of bits to represent particle distributions. In the lattice Boltzmann equation, a set of kinetic equations are solved in discrete space and discrete time. The lattice Boltzmann method is a finite-difference technique for solving the kinetic equation. The Navier–Stokes equation is obtained automatically in the long-wavelength and low-frequency limit. One crucial feature of the continuum description of the LBE method compared with original lattice gas models is that the LBE eliminates most of the noise of the system compared with the lattice gas method. This fact has been noted by several previous authors.[2,3] In addition, the LBE has considerable flexibility in the choice of the local equilibrium particle distribution. In contrast, the Fermi–Dirac equilibrium is the only distribution usually considered for the lattice gas automata. This additional freedom allows us to choose an equilibrium distribution to achieve desired physical properties, such as Galilean-invariant convection and a velocity-independent equation of state.[11]

Even though the LBE has been shown[12] to be an efficient numerical method for solving two-dimensional fluid problems and is considered to be an efficient and accurate numerical method for solving three-dimensional fluid problems, there has been no careful comparison with traditional numerical methods for two- and three-dimensional flows. The main objective of this paper is to describe a detailed implementation of the lattice Boltzmann method and to demonstrate the validity of the LBE method for three-dimensional benchmark problems. We hope to demonstrate the advantages and limitations of the LBE for real applications.

Section 2 is devoted to a review of the basic principles of lattice gas automata and the lattice Boltzmann approximation. The traditional lattice Boltzmann computational method is described, including the pressure-corrected lattice Boltzmann model, which maintains Galilean-invariant convection and the equation of state of an ideal gas.[11] Section 3 introduces a new version of the lattice Boltzmann method which only uses 14 directions instead of the usual 24 directions. This model is more efficient and memory-conserving than earlier models. In Section 4, typical three-dimensional fluid flows are simulated, including Beltrami flow, Green–Taylor vortex flows, and the decaying flows of three-dimensional isotropic

turbulence. Local and global quantities for both the lattice Boltzmann method and the spectral method are compared in detail. In the last section, a summary and discussion of limitations of the LBE are presented.

2. LATTICE BOLTZMANN METHOD FOR TWO- AND THREE-DIMENSIONAL FLUID FLOWS

2.1. Basic Principles of Lattice Gas Automata

The basic two-dimensional and three-dimensional lattice gas automata models[13,14] consist of identical particles moving on a regular lattice [hexagonal lattice in two dimensions and face-centered-hypercubic lattice (FCHC) in three dimensions]. The lattice unit c is unity for two dimensions and $\sqrt{2}$ for three dimensions. All particles have the same mass, momentum, and kinetic energy, and they reside only on the lattice vertices. There are b different particle momentum states allowed at each lattice site, associated with the directions to their nearest neighbors. An exclusion rule is usually imposed which requires that no more than one particle at a given site can have a given momentum. This exclusion rule is included in order to minimize memory requirements. If we use $N_a(\mathbf{x})$ $(a = 1,..., b)$ to denote the particle occupation in state a at site $\mathbf{x}$, then $N_a = 0$ or 1. There are two microscopic updating processes at each discrete time step: advection and collision. In the advection process, a particle in state $\mathbf{e}_a$ moves from its present site to the nearest neighbor site in the direction $\mathbf{e}_a$. In the collision process, particles at each site are redistributed among the b momentum states at the same site in such a way that the total particle number $(=\sum_{a=1}^{b} N_a)$ and the total momentum $(=\sum_{a=1}^{b} \mathbf{e}_a N_a)$ are conserved at each site. The microdynamical evolution of the lattice gas system is described exactly by the following microscopic equation:

$$N_a(\mathbf{x} + \mathbf{e}_a, t+1) = N_a(\mathbf{x}, t) + \Lambda_a \tag{1}$$

where Λ_a represents the collision operator, which includes the creation or annihilation of a particle in momentum state $\mathbf{e}_a$ and only depends on the information at the site $\mathbf{x}$ at time t. The collision operator has the form

$$\Lambda_a = \sum_{s,s'} (s' - s)\, P(s \to s') \prod_j N_j^{s_j} (1 - N_j^{s_j})^{1 - s_j} \tag{2}$$

where $s = (s_1, s_2,..., s_b)$ and s' represent the local states before and after collision. $P(s \to s')$ is the transition probability from state s to s'.

Particle and momentum conservation are satisfied if $\sum_{a=1}^{b} \Lambda_a = 0$ and $\sum_{a=1}^{b} \mathbf{e}_a \Lambda_a = 0$. The fluid density and momentum are defined as follows:

$$\begin{aligned} n(\mathbf{x}, t) &= \sum_a f_a(\mathbf{x}, t) \\ \mathbf{j}(\mathbf{x}, t) &= n\mathbf{v} = \sum_a f_a(\mathbf{x}, t)\, \mathbf{e}_a \end{aligned} \tag{3}$$

where

$$f_a(\mathbf{x}, t) = \langle N_a(\mathbf{x}, t) \rangle$$

and $\langle \cdots \rangle$ denotes an ensemble average.

If the microscopic collision transition probability P in (2) satisfies the semi-detailed balance condition

$$\sum_s P(s \to s') = 1$$

one can prove that the collisions will force the system to approach a local equilibrium described by the Fermi–Dirac distribution[13]:

$$f_a = \frac{1}{1 + \exp(\alpha + \beta \mathbf{e}_a \cdot \mathbf{v})} \tag{4}$$

where α and β are Lagrange multipliers determined by mass and momentum conservation.

Assuming $L \gg 1$ and $T \gg 1$, where T is the macroscopic characteristic time and L is a characteristic length, one obtains from (1) the continuum version of the kinetic equation:

$$\partial_t f_a + \mathbf{e}_a \cdot \nabla f_a = \Omega_a \tag{5}$$

where Ω is the collision operator obtained by replacing N_a by f_a in Λ. After ensemble averaging the microscopic equation, and using a Chapman–Enskog expansion, it can be shown that the system approximates the following fluid equations[1,13]:

$$\begin{aligned} \partial_t n + \nabla \cdot (n\mathbf{v}) &= 0 \\ \partial_t (n\mathbf{v}) + \nabla \cdot [ng(n)\, \mathbf{vv}] &= -\nabla p + \nu \nabla^2 (n\mathbf{v}) \\ p &= \tfrac{1}{2}[n - g(n)\, \mathbf{v}^2] \end{aligned} \tag{6}$$

where $g(n)$ is a function of density which should be unity, but it is not unity for lattice gas models. This causes non-Galilean effects to appear. The

incompressible Navier–Stokes equations are recovered only in the low-Mach-number limit when time, pressure, and viscosity are rescaled by the factor g. Because $g(n)$ depends on density, this rescaling is consistent only for problems which have nearly constant density.

2.2. A Pressure-Corrected Lattice Boltzmann Method with a Single-Time Relaxation

We will describe a pressure-corrected lattice Boltzmann model proposed recently by Chen *et al.*[11] This model approximates the Navier–Stokes equations in the long-wavelength and low-frequency limit.

In general, we consider N-dimensional physical problems on D-dimensional lattices with b different allowed moving directions and one rest state. For two-dimensional flows, $D=2$ and $b=6$ (hexagonal lattice). For three-dimensional flows, $D=4$ and $b=24$ (the face-centered hypercubic lattice, FCHC). The Boltzmann equation for this model is given by

$$f_i(\mathbf{x}+\mathbf{e}_i, t+1)=f_i(\mathbf{x}, t)+\Omega_i(f(\mathbf{x}, t)), \qquad i=0, 1,..., b \tag{7}$$

where $\Omega_i=\Omega(f(\mathbf{x}, t))$ is a local collision operator, f_i is a single-particle distribution function. $|\mathbf{e}_i|=c$ is the lattice unit length as discussed above. In the previous section, we saw that Fermi–Dirac statistics are required and f_i is restricted to be in a range bounded by zero and one. For the lattice Boltzmann method, the particle distribution does not have an upper bound in general. To be consistent with particle distribution, we enforce a Maxwell-type equilibrium distribution and require that $f_i \geqslant 0$.

Assuming that this distribution can be expanded about its local equilibrium value,

$$f_i=f_i^{\mathrm{eq}}+f_i^{\mathrm{neq}}, \qquad \frac{|f_i^{\mathrm{neq}}|}{|f_i^{\mathrm{eq}}|}\ll 1 \tag{8}$$

the collision operator becomes

$$\Omega_i(f)=\Omega_i(f^{\mathrm{eq}})+\frac{\partial \Omega_i(f^{\mathrm{eq}})}{\partial f_j} f_j^{\mathrm{neq}}+O(|f^{\mathrm{neq}}|^2) \tag{9}$$

Chapman–Enskog theory requires $\Omega_i(f^{\mathrm{eq}})=0$. Neglecting higher-order terms, we have the linearized form of the collision operator:

$$\Omega_i(f)=M_{ij} f_j^{\mathrm{neq}}$$

Here, $M_{ij}=\partial\Omega_i(f^{\mathrm{eq}})/\partial f_j$. If we further assume that the local particle distribution relaxes to equilibrium state at a single rate, $\partial\Omega_i/\partial f_j=-(1/\tau)\,\delta_{ij}$, with time scale τ,[11] we arrive at the following linearized form:

$$\Omega_i=\frac{-1}{\tau}(f_i-f_i^{\mathrm{eq}}) \tag{10}$$

Note that we have both $\sum_i \Omega_i=0$ and $\sum_i \mathbf{e}_i\Omega_i=0$. In order for the fluid to have Galilean-invariant convection and a pressure which does not depend upon velocity, the following equilibrium distribution f_i^{eq} is assumed:

$$f_i^{\mathrm{eq}}=d+\frac{\rho D}{c^2 b}\mathbf{e}_i\cdot\mathbf{v}+\rho\frac{D(D+2)}{2c^4 b}(\mathbf{e}_i)_\alpha(\mathbf{e}_i)_\beta u_\alpha u_\beta-\frac{\rho D}{2c^2 b}\mathbf{v}^2 \tag{11}$$

$$f_0^{\mathrm{eq}}=d_0-\frac{\rho}{c^2}\mathbf{v}^2 \tag{12}$$

In the above equations, d_0 is the average particle number. The particle density per site ρ and the fluid velocity $\mathbf{v}$ are defined by

$$\rho=\sum_i f_i \qquad \text{and} \qquad \rho\mathbf{v}=\sum_i \mathbf{e}_i f_i \tag{13}$$

In (11),

$$d=(\rho-d_0)/b$$

Performing a Taylor expansion in time and space and taking the long-wave length and low-frequency limit, we obtain the continuum form of the kinetic equation up to second order:

$$\partial_t(f_i)+\mathbf{e}_i\cdot\nabla f_i+\tfrac{1}{2}\mathbf{e}_i\mathbf{e}_i:\nabla f_i+\mathbf{e}_i\cdot\nabla\partial_t(f_i)+\tfrac{1}{2}\partial_t^2(f_i)=\Omega_i \tag{14}$$

The momentum equation can be written as

$$\partial_t(\rho\mathbf{v})+\nabla\cdot\Pi=0$$

with the momentum flux tensor Π of the form

$$\Pi_{ab}=\sum_i(\mathbf{e}_i)_a(\mathbf{e}_i)_b f_i$$

Using the Chapman–Enskog expansion, one obtains

$$\Pi_{ab}=\Pi_{ab}^{(0)}+\Pi_{ab}^{(1)}$$

with the stress tensor $\Pi_{ab}^{(0)}=\sum_i(\mathbf{e}_i)_a(\mathbf{e}_i)_b f_i^{\mathrm{eq}}$ and $\Pi_{ab}^{(1)}=(\mathbf{e}_i)_a(\mathbf{e}_i)_b f_i^{\mathrm{neq}}$.

After simple algebra, one obtains

$$\Pi_{ab}^{(0)} = \rho u_a u_b + \frac{bc^2 d}{D}\,\delta_{ab}$$

$$\Pi_{ab}^{(1)} = -\frac{c^2(2\tau-1)}{2(D+2)}\,\rho\dot{\gamma}_{ab} + \left[\frac{c^2\tau}{D} - \frac{c^2(2\tau-1)}{2(D+2)}\right]\nabla\cdot(\rho\mathbf{v})\,\delta_{ab} \tag{15}$$

where $\dot{\gamma}_{ab}$ is the time-rate-of-strain tensor, defined by

$$\dot{\gamma}_{ab} = \frac{\partial u_a}{\partial x_b} + \frac{\partial u_b}{\partial x_a}$$

Equation (15) can be written as a relation between the stress tensor τ and the rate-of-strain tensor:

$$\tau_{ab} = -\frac{c^2(2\tau-1)}{2(D+2)}\,\rho\dot{\gamma}_{ab} + \left[\frac{c^2\tau}{D} - \frac{c^2(2\tau-1)}{2(D+2)}\right]\nabla\cdot(\rho\mathbf{v})\,\delta_{ab} \tag{15'}$$

For incompressible fluids, $\Pi_{ab}^{(1)}$ can be written

$$\Pi_{ab}^{(1)} = -\frac{c^2(2\tau-1)}{2(D+2)}\,\dot{\gamma}_{ab}$$

and the Navier–Stokes equations become

$$\begin{aligned} \partial_t(\rho) + \nabla\cdot(\rho\mathbf{v}) &= 0 \\ \partial_t(\rho\mathbf{v}) + \nabla\cdot(\rho\mathbf{v}\mathbf{v}) &= -\nabla p + \mu\nabla^2(\rho\mathbf{v}) \end{aligned} \tag{16}$$

In the above equations, p is the pressure, $p = c^2\rho/D$, and μ is the shear viscosity. The kinematic viscosity $\nu = \mu/\rho$ can be written simply as

$$\nu = \nu_c + \nu_p = \frac{c^2(2\tau-1)}{2(D+2)} \tag{17}$$

where ν_c and ν_p are the viscosities induced by collisions and propagation, respectively. Note that in our present single-relaxation-time model, the kinematic viscosity only depends on the relaxation time, not on local density. This is a distinct advantage over traditional LBE methods for simulating incompressible fluids.

For most previous simulations in three dimensions both in lattice gas and lattice Boltzmann schemes, a 24-moving-direction lattice in four-dimensional space (the FCHC lattice) has to be used in order to maintain isotropy of the stress tensor required by fluid equations. This lattice has

Cartesian coordinates $(\pm 1, \pm 1, 0, 0)$, $(\pm 1, 0, \pm 1, 0)$, $(\pm 1, 0, 0, \pm 1)$, $(0, 0, \pm 1, \pm 1)$, $(0, \pm 1, 0, \pm 1)$, and $(0, 0, \pm 1, \pm 1)$. The projection of lattice dynamics into three-dimensional space produces the expected three-dimensional fluid flows. In order to save computational memory and obtain most efficiency for three-dimensional flows, a periodic condition for the lattice length in the fourth dimension is commonly assumed. Therefore, this lattice is equivalent to a two-speed lattice in three-dimensional space with speeds $\sqrt{2}$ and 1. The fourth dimensional coordinate is either 0 or ± 1, respectively. For lattice Boltzmann simulations it is not necessary to write out all the moving directions when they have different coordinates in the fourth dimensions. The only quantities required are the particle speeds in three dimensions. From Eq. (11), we see that the particles moving along same coordinate in the first three dimensions but with different moving direction in the fourth direction have the same equilibrium distributions. This is equivalent to doubling the particle distribution along the axes while neglecting the fourth dimensional coordinates. Thus the original FCHC lattice can be replaced an 18-moving-directional lattice with two speeds. This reduction saves about 25% in memory requirements and 25% in computer speed.

3. A NEW LATTICE BOLTZMANN METHOD FOR THREE-DIMENSIONAL FLUID FLOWS WITH FOURTEEN MOVING DIRECTIONS

In the previous section, we discussed the relation between FCHC model and a lattice Boltzmann model with 18 moving directions. In this section, we introduce a new three-dimensional lattice with only 14 particle moving directions. We prove that the related lattice Boltzmann method approximates the usual three-dimensional hydrodynamic equations. By changing from 24 to 14 directions, the method becomes 42% more efficient.

We consider a cubic lattice in three dimensions and choose the new set of lattice vectors associated with the moving directions of the particles as follows: $(\pm 2, 0, 0)$, $(0, \pm 2, 0)$, $(0, 0, \pm 2)$, and $(\pm 1, \pm 1, \pm 1)$. Let us call the speed two lattice a class I lattice and the remainder as a class II lattice. Using simple group analysis,[14] we write the lattice symmetry properties

$$\sum_a (\mathbf{e}_a)_i (\mathbf{e}_a)_j = c^2 \frac{M}{D} \delta_{ij} \tag{18}$$

where c^2 is 4 for the class I and 3 for class II, M is 6 for the class I and 8 for the class II, and D is 3 (dimensions) for both cases.

We also have

$$\begin{aligned} &\sum_a (\mathbf{e}_a)_i (\mathbf{e}_a)_j (\mathbf{e}_a)_k (\mathbf{e}_a)_l = 32\delta_{ijkl} && \text{for class I} \\ &\sum_a (\mathbf{e}_a)_i (\mathbf{e}_a)_j (\mathbf{e}_a)_k (\mathbf{e}_a)_l = 8\Delta_{ijkl} - 16\delta_{ijkl} && \text{for class II} \end{aligned} \tag{19}$$

where $\Delta_{ijkl} = \delta_{ij}\delta_{kl} + \delta_{ik}\delta_{jl} + \delta_{il}\delta_{jk}$ and $\delta_{ijkl} = 1$ for $i = j = k = l$ and 0 for all others.

The kinetic equation (7) can be rewritten as

$$f_i(\mathbf{x} + \mathbf{e}_i, t+1) - f_i(\mathbf{x}, t) = -\frac{f_i - f_i^{\text{eq}}}{\tau}, \qquad i = 0, 1, \ldots, 14 \tag{7'}$$

We choose the equilibrium distribution function as follows:

$$\begin{aligned} f_i^{(1)\,\text{eq}} &= d^{(1)} + \alpha^{(1)}\mathbf{e}_i^{(1)} \cdot \mathbf{v} + c_1^{(1)}(\mathbf{e}_i \cdot \mathbf{v})^2 + c_2^{(1)}u^2 \\ f_i^{(2)\,\text{eq}} &= d^{(2)} + \alpha^{(2)}\mathbf{e}_i^{(2)} \cdot \mathbf{v} + c_1^{(2)}(\mathbf{e}_i \cdot \mathbf{v})^2 + c_2^{(2)}u^2 \\ f^{(0)\,\text{eq}} &= d^{(0)} + \gamma u^2 \end{aligned} \tag{20}$$

where the superscripts (1), (2), and (0) refer to the class I, class II, and rest particles. From conservation of mass and momentum in (13), we obtain a relation between the undetermined coefficients in (20):

$$\begin{aligned} 6d^{(1)} + 8d^{(2)} + d^{(0)} &= n \\ 8c_1^{(1)} + 6c_2^{(1)} + 8c_1^{(2)} + 8c_2^{(2)} + \gamma &= 0 \\ 8(\alpha^{(1)} + \alpha^{(2)}) &= n \end{aligned} \tag{21}$$

Similar to the first equation in (15), we have the zeroth order of the stress tensor:

$$\begin{aligned} \pi_{ij}^{(0)} = &\left[8(d^{(1)} + d^{(2)}) + 8(c_2^{(1)} + c_2^{(2)})\, u^2\right] \delta_{ij} \\ &+ \left[(32c_1^{(1)} - 16c_1^{(2)})\, \delta_{ijkl} + 8c_1^{(2)}\Delta_{ijkl}\right] u_k u_l \end{aligned}$$

In order to maintain an isotropic stress tensor and an ideal gas equation of state, we require that

$$c_1^{(1)} = \frac{n}{32}, \qquad c_1^{(2)} = \frac{n}{16}$$

$$c_2^{(1)} = -\frac{n}{48}, \qquad c_2^{(2)} = -\frac{n}{24}$$

From (21), we have

$$\gamma = -\frac{7n}{24}$$

For simplicity, we choose

$$d^{(1)} = \tfrac{1}{2}d^{(2)} = d^{(0)}$$

Therefore, we have a simple expression for $\pi_{ij}^{(0)}$:

$$\pi_{ij}^{(0)} = \tfrac{24}{23}n\delta_{ij} + nu_i u_j$$

The sound speed of this system is $(24/23)^{1/2}$. To obtain the Navier–Stokes equation, we calculate to first order in the stress tensor:

$$\pi_{ij}^{(1)} = \sum_a (\mathbf{e}_a)_i (\mathbf{e}_a)_j f_a^{(1)} = -\tau \sum_a (\mathbf{e}_a)_i (\mathbf{e}_a)_j \left[\frac{\partial f_a^{(0)}}{\partial t} + (\mathbf{e}_a)_k \frac{\partial f_a^{(0)}}{\partial x_k} \right]$$

If we assume $\alpha^{(2)} = 2\alpha^{(1)}$, from the last equation in (22), we obtain

$$\alpha^{(1)} = \frac{n}{24}$$

$$\alpha^{(2)} = \frac{n}{12}$$

The first-order stress tensor has the form

$$\pi_{ij}^{(1)} = \frac{-2\tau}{3}\left(\frac{\partial nu_i}{\partial x_j} + \frac{\partial nu_j}{\partial x_i}\right) + \frac{26\tau}{69}\delta_{ij}\nabla \cdot (n\mathbf{v})$$

Taking into consideration the convective transport coefficients as before in (17), we obtain the Navier–Stokes equation for this new model:

$$\frac{\partial nu_i}{\partial t} + \frac{\partial nu_i u_j}{\partial x_j} = -\frac{\partial p}{\partial x_i} + \nu \frac{\partial^2 nu_i}{\partial x_j^2} + \eta \frac{\partial}{\partial x_i}\nabla \cdot (n\mathbf{v}) \tag{22}$$

with the kinematic viscosity $\nu = (2\tau - 1)/3$ and the bulk viscosity $\eta = 2\tau/3 - 136/87$.

In order to have a correct equation of state, we use a rest particle state for the present 14-moving-direction lattice Boltzmann model. It is not necessary to keep this rest-particle number state, because of the freedom in the equilibrium distribution function in (20). By adjusting the parameter in Eqs. (21), one can also obtain a correct fluid equation using 14 moving directions only.[15]

The lattice we are using now has a particle speed 2 along x, y, z axis directions. It could be a unit speed. This requires the particle equilibrium distributions in these directions to be eight times bigger than those in the diagonal directions in order to have the isotropic property for the stress tensor. In order to make the particle distribution in all directions close to an isotropic distribution, we prefer to use the speed-two lattice model. The speed-two lattice is the preferable model for the periodic problems described in the next section. For the problems with arbitrarily complicated boundaries, it may be easier to use the speed-one lattice, for which we only need to treat one lattice layer as the walls by the bouncing back of particles.

4. THREE-DIMENSIONAL SIMULATIONS WITH PERIODIC BOUNDARIES

In order to test the accuracy and efficiency of the new method, we present in this section direct numerical simulation results and compare them with results obtained using the spectral method, a very efficient method for the periodic boundary conditions.

4.1. Beltrami Flow and the Measurement of Kinematic Viscosity

Considering the incompressible limit of the lattice Boltzmann model, the three-dimensional Navier–Stokes equation in (22) can be written in the form

$$\frac{\partial \mathbf{v}}{\partial t} + \omega \times \mathbf{v} = -\nabla\left(\frac{p}{n} + \frac{u^2}{2}\right) - \nu \nabla \times \omega \tag{23}$$

where $\omega = \nabla \times \mathbf{v}$ is the vorticity. For Beltrami flows, $\mathbf{v} \times \omega = 0$. In periodic boundaries, $\nabla^2(p + u^2/2) = 0$, and the above equation has an exponentially decaying solution:

$$\frac{\partial \mathbf{v}}{\partial t} = -\nu \nabla \times \omega \tag{24}$$

Assume there is a vector potential ψ having the following relation to velocity:

$$\mathbf{v} = \nabla \times \psi \mathbf{e} + \frac{1}{\lambda} \nabla \times (\nabla \times \mathbf{e}\psi)$$

One can easily show that $\omega = \lambda \mathbf{v}$. Therefore, if we initially assume that

$$\psi = \sin(\lambda \cdot \mathbf{x})$$

we have an exponentially decaying velocity solution for (24):

$$\mathbf{v}(\mathbf{x}, t) = \mathbf{v}(\mathbf{x}, 0) \exp(-\lambda^2 \nu t) \tag{25}$$

By measuring the decay rate at any spatial point, one can obtain the kinematic viscosity ν. By simulating Beltrami flows, a simple check of the accuracy of the lattice Boltzmann scheme is that it maintains the required $\mathbf{v} \times \omega = 0$.

This simulation has been done using both the 18-direction lattice Boltzmann model and the 14-direction lattice Boltzmann model. But in this paper, we will only show the results from the 14-direction model. The system size for the simulation was $64 \times 64 \times 64$. In order to see the basic property of the Beltrami flow, we have measured the time evolution of $\langle (\mathbf{v} \times \omega)^2 \rangle$. Here $\langle \cdots \rangle$ denotes the spatial average. We have obtained correctly the basic Baltrami flow property: $\langle (\mathbf{v} \times \omega)^2 \rangle = 0$ throughout simulation.

In Fig. 1 we present the total energy decay as a function of time for different values of relaxation time τ. We see that the decay for different relaxation times satisfies the exponential rule with different decay rates. This is exactly described by the decay equation in (25).

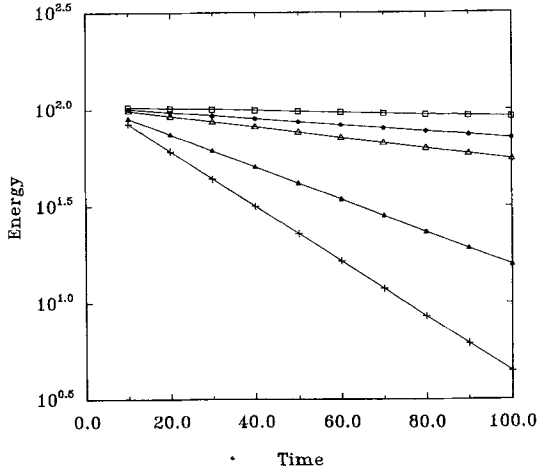

Fig. 1. Energy decay as a function of time for different relaxation times τ ranging from 0.6 to 3.0: (□) $\tau = 0.6$; (●) $\tau = 0.8$; (△) $\tau = 1.0$; (▲) $\tau = 2.0$; (+) $\tau = 3.0$. The exponential decay of energy demonstrates that the kinematic viscosity is constant for a given τ. The slope determines the kinematic viscosity.

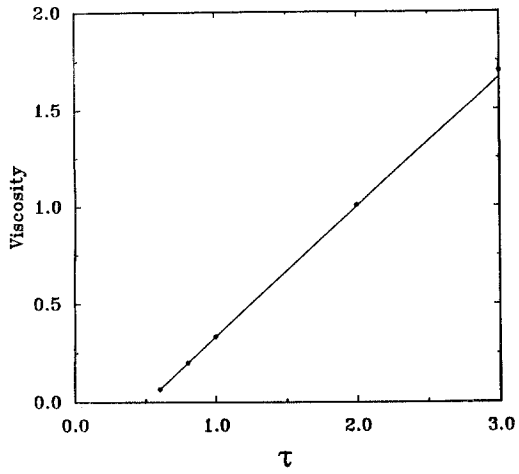

Fig. 2. Comparison of the kinematic viscosity as a function of relaxation time: theoretical analysis (solid line) and numerical simulation (dots). The theoretical result is obtained using the standard Chapman–Enskog expansion. The measurements are obtained from the energy decay of the Beltrami flow.

As discussed in the Section 2, the kinematic viscosity only depends on the relaxation time. By measuring the energy (or velocity) decay rate, we could accurately obtain the relation between the time relaxation parameter τ and the kinematic viscosity. In Fig. 2, we present the theoretical prediction of viscosity and numerical measurements of the kinematic viscosity for the 14-direction model (dots). We see that when the τ is smaller than 1, the theoretical results agree very well with actual numerical measurements (at least four significant figures compared with the analytic results). For larger values of τ the error increases. This is possibly due to the fact that the relaxation characteristic time is comparable with the real macroscopic simulation time. Therefore, the Chapman–Enskog expansion will be valid only in the low-order approximation.

As discussed in ref. 16, the linear stability of the single-time relaxation lattice Boltzmann method requires that $\tau > 1/2$. Therefore, we only make comparisons for τ satisfing this condition.

4.2. The Decaying Taylor–Green Vortex: Time-Dependent Properties and Vortex Structure

Taylor–Green vortex flow and the time evolution of its statistical quantities have been extensively studied.[17–19] The Taylor–Green vortex has been of continuing interest as a numerical test not only because its flow pattern is simple, but also because it has a turbulent decay mechanism

which produces small eddies and which enhances dissipation by the stretching of vortex lines.

To compare our lattice Boltzmann method with the spectral method, we have to scale the kinetic equaton (7). That is, we have to use physical space and time units for the lattice Boltzmann calculations. To do this, we assume that one unit lattice length is equal to a real space distance Δx and a lattice time unit is equal to a real time Δt. Then the Navier–Stokes equation (22) in lattice units can be rescaled using $t^* = t\,\Delta t$ and $x^* = x\,\Delta x$. Here t is the lattice unit and t^* is the physical unit; x is the lattice unit and x^* is the physical unit. Assume that the velocity ratio between the lattice system and the real system is $\lambda = u_{\mathrm{LBE}}/u_{\mathrm{real}}$ and the length scale ratio $\eta = L_{\mathrm{LBE}}/L_{\mathrm{real}}$. Then the time scale is η/λ. The viscosity scale ratio is λ/η. Using these scalings, we can relate the lattice Boltzmann results to results from the spectral method.

A spectral code for simulating three-dimensional isotropic turbulent flows in the periodic condition was developed. In Fourier space, the incompressible Navier–Stokes equation can be written as

$$\frac{\partial \mathbf{v}_k}{\partial t} = \mathbf{P}(\mathbf{k}) \cdot (\mathbf{v} \times \omega)_{\mathbf{k}} - \nu k^2 \mathbf{v}_k \tag{26}$$

where the tensor $\mathbf{P}$ is the projection on the space of solenoidal fields, defined as

$$\mathbf{P}_{ij}(\mathbf{k}) = \delta_{ij} - \frac{k_i k_j}{k^2}$$

A pseudospectral method was used to calculate the nonlinear term on the right-hand side of (26). The time integration utilized an Adams–Bashforth method with the initial step employing a modified Euler method. The viscosity term is exactly integrated. The complete time evolution of the spectral method can written as follows:

$$\frac{\mathbf{v}_{\mathbf{k}}^{n+1} - \mathbf{v}_{\mathbf{k}}^{n} \exp(-\nu k^2\,\Delta t)}{dt}$$

$$= \mathbf{P}(\mathbf{k}) \cdot \left[\tfrac{3}{2}(\mathbf{v} \times \omega)_{\mathbf{k}}^{n} \exp(-\nu k^2\,\Delta t) - \tfrac{1}{2}(\mathbf{v} \times \omega)_{\mathbf{k}}^{n-1} \exp(-2\nu k^2\,\Delta t)\right]$$

In both the lattice Boltzmann and the spectral methods, a lattice size of $128 \times 128 \times 128$ was used. We chose the following initial velocity distribution for the Taylor–Green vortex:

$$\begin{aligned} v_x(\mathbf{x}, 0) &= v_0 \cos x \sin y \cos z \\ v_y(\mathbf{x}, 0) &= -v_0 \sin x \cos y \cos z \\ v_z(\mathbf{x}, 0) &= 0 \end{aligned} \tag{27}$$

where $v_0 = 1$ for the spectral method, which has a periodicity 2π in all directions, and $v_0 = 0.2$ for lattice Boltzmann method with periodicity 128 in all directions. Also, in the spectral simulation, we use a viscosity of 0.05 for simulations of a Reynolds number of 200 and a viscosity of 0.0333 for simulations of a Reynolds number of 300. In the lattice Boltzmann simulation, we use the viscosities of 0.0203718 and 0.0135812 to obtain the corresponding Reynolds numbers. Using these parameters, one lattice time unit equals 0.01 unit of spectral simulation time. In Fig. 3, we plot the evolution

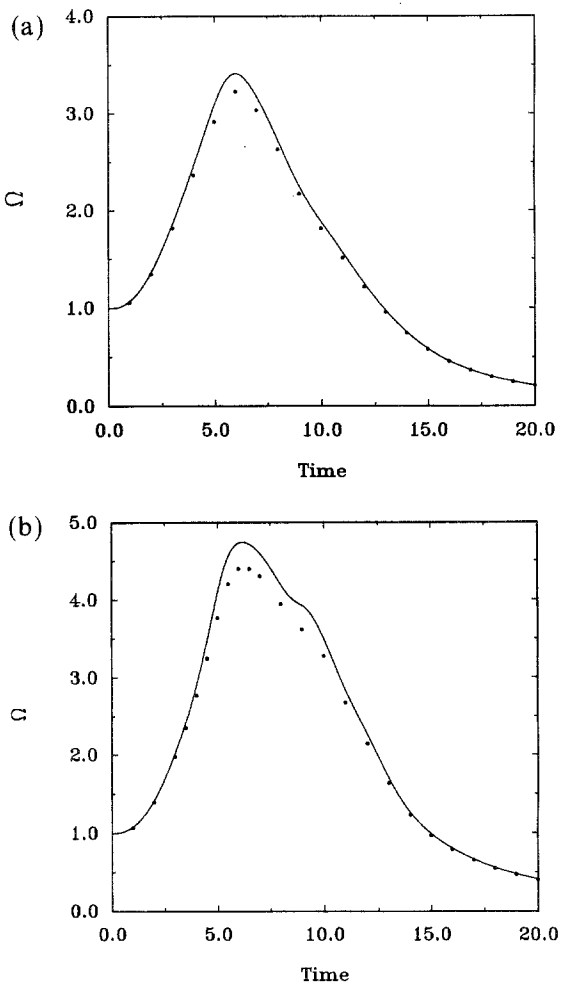

Fig. 3. Enstrophy Ω versus time: (a) Re = 200; (b) Re = 300. Solid lines are results from the spectral method. The circles are lattice Boltzmann results.

of the enstrophy, defined as $\langle \Omega \rangle = \langle \omega^2 \rangle$, at (a) Re = 200 and (b) Re = 300 for the time interval from 0 to 20, where $\langle \cdots \rangle$ represents the spatial average. If there were no nonlinear terms, $\langle \Omega \rangle$ would have a monotonic decay. The increase of the $\langle \Omega \rangle$ with time illustrates the existence of vortex stretching in the Taylor–Green vortex. We found that for both cases (Re = 200 and Re = 300), the lattice Boltzmann method and spectral method agree well in the initially increasing region when the nonlinear term dominates and at later times when the dissipation mechanism dominates. For the region near the peak of $\langle \Omega \rangle$, there is about 5–10% difference between these two methods. This is probably due to the following two reasons: first, the spectral method is solving the exact incompressible Navier–Stokes equations directly, while the lattice Boltzmann method we have developed in this paper is actually solving the incompressible fluid limit of the compressible fluid flows at low Mach number. The compressible effect will be strongest when the nonlinear term and the dissipation term are comparable. Second, the lattice Boltzmann scheme in the present paper is first order in time and second order in space. The existence of higher-order terms in the discrete approximation of the continuum version of the kinetic equation (14) may cause some numerical effects. From Figs. 3a and 3b we also found that the smaller Reynolds number gives better agreement between the spectral method and the lattice Boltzmann method. This is due to the nonlinear interaction term playing a more important role at high Reynolds numbers than at low Reynolds numbers. In Figs. 4 and 5 we present the time evolution of the relative energy change

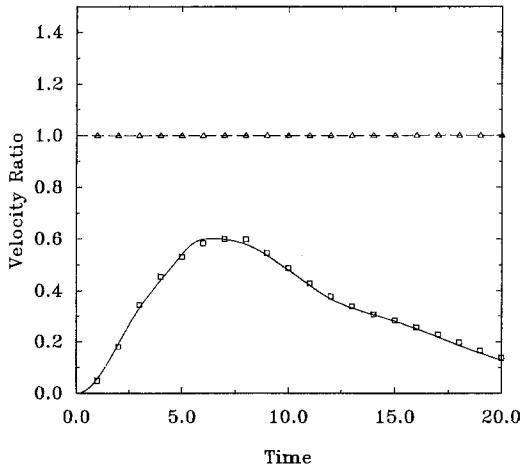

Fig. 4. Relative energy as a function of time. $\langle v_y^2 \rangle / \langle v_x^2 \rangle$: the dashed line represents the spectral method and the triangles represent the lattice Boltzmann results; $\langle v_z^2 \rangle / \langle v_x^2 \rangle$: the solid line is the result of the spectral method and the squares indicate lattice Boltzmann results.

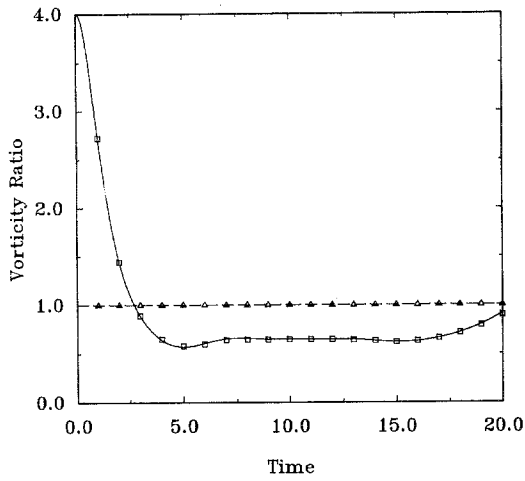

Fig. 5. Relative vorticity squared as a function of time. $\langle\omega_y^2\rangle/\langle\omega_x^2\rangle$: the dashed line represents spectral results and the triangles represent lattice Boltzmann results; $\langle\omega_z^2\rangle/\langle\omega_x^2\rangle$: the solid line represents spectral results and the squares represent lattice Boltzmann results.

and the relative vorticity change: $\langle v_y^2\rangle/\langle v_x^2\rangle$, $\langle v_z^2\rangle/\langle v_x^2\rangle$, $\langle\omega_y^2\rangle/\langle\omega_x^2\rangle$, and $\langle\omega_z^2\rangle/\langle\omega_x^2\rangle$ for both the spectral simulations and the lattice Boltzmann calculations. We found that even though the relative energy and vorticity changes are very complicated with the evolution of time, the lattice Boltzmann scheme is capable of tracking the main properties of anisotropic energy dissipation and energy decay. Because of the symmetry of the initial velocity and vorticity in the x and y directions, the energy and enstrophy ratio of these two directions are constants. The initial velocity in the z direction is zero, but the nonlinear interaction term in Eq. (23) transfers energy from the x and y directions to the z direction. In contrast, the initial vorticity in the z direction is bigger than that in the other directions. With the evolution of time, the vorticity intensity distributions in all three directions are more isotropic and are almost equal when $t = 20$.

In order to compare three-dimensional vortex structures, we plot in Fig. 6 velocity contours for a cross section ($z = 64$) at times $t = 4$ and $t = 10$. At $t = 4$, the nonlinear interaction term dominates and the vortex structure is being stretched. The enstrophy is increasing. At $t = 10$, the main feature is dissipation. At this moment, the Taylor microscopic Reynolds number is quite small and the local vortex structure is slowly decaying. We see that the vortex structures generated by the lattice Boltzmann method agree with the spectral method results. We also found that the same vortex structures agree along different planes and at other times.

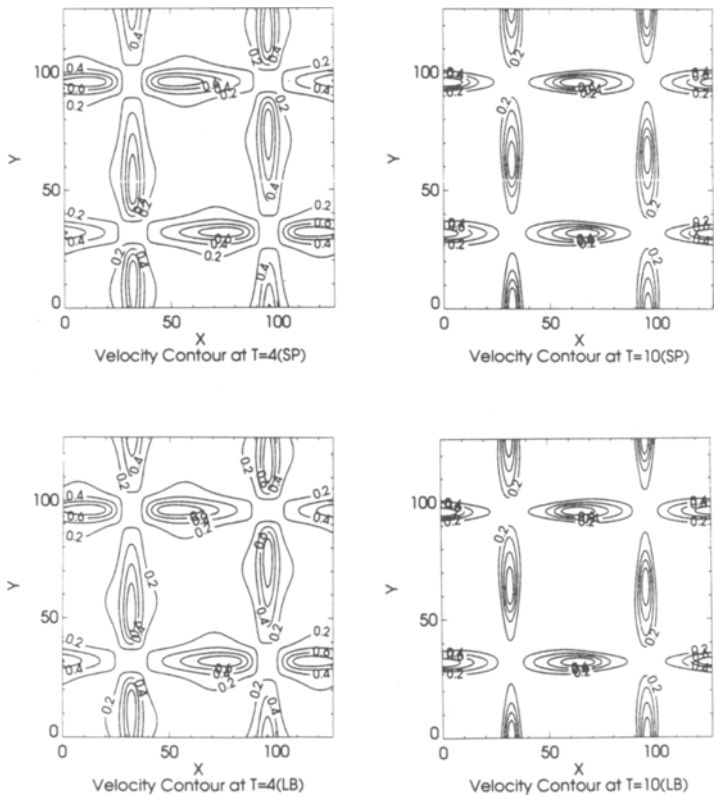

Fig. 6. Comparisons between the spectral method (SP) and the lattice Boltzmann (LB) simulations for the velocity contour lines at $z = 64$. The left plots are at $t = 4$ and the right plots are at $t = 10$. The similar velocity structures for different time steps can be clearly seen from the plots. This demonstrates that the two numerical schemes agree well not only globally, but also locally.

4.3. Three-Dimensional Isotropic Turbulence

In this section, we present briefly some comparisons for the simulations of three-dimensional isotropic decaying turbulence by the spectral method and the lattice Boltzmann method. The system size used in this section is $128 \times 128 \times 128$ lattice units.

The initial value of the velocity $\mathbf{v}(\mathbf{k}, 0)$ for the spectral code is chosen from a Gaussian random distribution,[20] which gives the energy spectrum

$$E(k) = 16(2/\pi)^{1/2} u_0^2 k_0^{-5} k^4 \exp[-2(k/k_0)^2]$$

where the energy spectrum is defined as

$$E(k) = \tfrac{1}{2} \sum_{S(k)} |\mathbf{v}(\mathbf{k}')|$$

The summation $\sum_{S(k)}$ extends over one shell in k space: $k \leqslant |\mathbf{k}'| < k+1$. Here $u_0 = 1$ is the initial rms velocity and the peak wavenumber is $k_0 = 4.75683$. The viscosity of the system is 0.01189, corresponding to an initial Taylor microscopic Reynolds number $R_\lambda = 56$. This has an eddy turnover time of 0.45. Because the lattice Boltzmann method solves the Navier–Stokes equations directly in physical space and in order to have a same initial velocity field, we transfer the velocity distribution in k space to physical space as an initial condition.

In Fig. 7, we present two time steps ($t = 0$ and $t = 1$) for the energy spectra in k space calculated from the spectral method (solid lines) and lattice Boltzmann method (diamonds). They agree very well at low wavenumbers. For high wavenumbers, there are some discrepancies between these two methods. This indicates that the current method accurately predicts an energy decay, but does not capture the high-order dissipation spectra (not shown in this paper). In a forthcoming paper,[21] we will

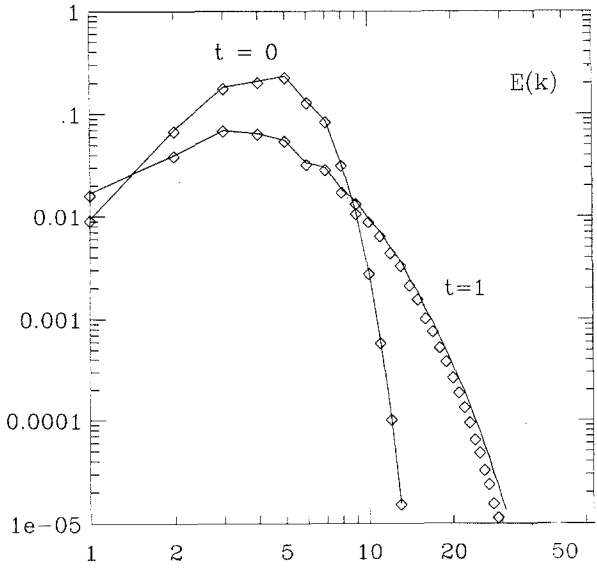

Fig. 7. Energy spectra for three-dimensional decaying isotropic turbulence from the spectral method (solid lines) and the lattice Boltzmann method (diamonds) at times $t = 0$ and $t = 1$. The lattice Boltzmann method tracks the important properties of the spectrum in the low-k region.

present more detailed calculations for three-dimensional turbulent flows with additional comparisons between the spectral method and the lattice Boltzmann method.

Another interesting case in turbulent flows is forced three-dimensional isotropic turbulence, which can also be simulated using the lattice Boltzmann method. A major challenge is the forcing technique. Usually, to have a stable spectrum in k space, in most spectral simulationss[22] a low wave constant force is used to maintain a constant energy.[23] To obtain the same velocity distribution as the spectral method, one can transfer this forcing to x space by adding some low wave mode forcing[12] directly.

5. CONCLUDING REMARKS

In this paper, we have described two lattice Boltzmann computational models for three-dimensional fluid flows, based on the linearized Boltzmann approximation with a single time relaxation. We demonstrate that the new 14-direction lattice Boltzmann model requires less storage and computational time for solving real three-dimensional problems as compared with previous lattice Boltzmann methods. Since there is no isotropic single-speed lattice model in three dimensions which produces an isotropic stress tensor, a two-speed lattice must be used. It appears that the current 14-direction lattice Boltzmann model has possibly the least number of directions required for three-dimensional isotropy.

The present lattice Boltzmann model utilizes a new equilibrium distribution function, which leads to a correct equation of state and which has a Galilean-invariant convection term. The numerically measured viscosity agrees well with the theoretical analysis of this model. In principle, the current model could give an arbitrarily small viscosity. Numerical tests show that the hydrodynamic system is stable for small viscosities. For a system with $128 \times 128 \times 128$ lattice sites, we conclude from numerical experience that the smallest viscosity which could be used is about 0.001. This allows a Reynolds number of about 1000. For higher Reynolds numbers, the system energy oscillates. In this low-viscosity region, we are not convinced that the lattice Boltzmann scheme presented in this paper correctly models incompressible Navier–Stokes flows. Also, we are not sure at this moment of the exact cause of this instability.

The lattice-Boltzmann simulations of several basic three-dimensional fluid flows and isotropic turbulence in a periodic geometry presented in this paper show good agreement with the spectral method for several tests, including the time evolution of energy, enstrophy decay, and vortex evolution in space. The time evolution of spectra for three-dimensional isotropic

fluid flows also compare well with spectral calculations. This demonstrates that the lattice Boltzmann method could be an alternative method for studying the isotropic turbulence. The simulation speed of the current lattice Boltzmann model is about 2.5 times faster than the spectral code we developed for the CM-2. We believe that our current CM-2 spectral code has almost obtained the maximum computer speed possible on the current CM-2. In our spectral code, about 98% of the computational time is spent in the FFT. This part of the code is fully optimized. The current lattice Boltzmann code requires 18 three-dimensional arrays to store the particle distribution information and temporary arrays. The spectral code only requires about 12 arrays. Hence, the spectral code requires 30% less memory. Thus, on one-quarter of a CM-2 (16k processors), the spectral code could run a system of $512 \times 256 \times 256$, while the current Boltzmann method can only run $256 \times 256 \times 256$. On the other hand, even though the spectral method could solve the three-dimensional problems with periodic geometry quite efficiently, spectral methods for complicated geometry have not yet been developed. Hence the lattice Boltzmann method is the only known method for solving problems such as flows through porous media.[7,8]

Although the present lattice Boltzmann method produces accurate results compared with spectral method, the lattice Boltzmann kinetic equation is a numerical scheme of the first order in time and second order in space. This can be see from the discretized kinetic equation (14). The equation we want to solve is the continuum version of the kinetic equation (14). In order to increase accuracy both in time and space, it would be desirable to develop a higher-order lattice Boltzmann scheme.

We conclude that the lattice Boltzmann method could be an alternative numerical method for solving the Navier–Stokes equations for three-dimensional problems in both periodic and complicated geometries. The parallel nature of the lattice Boltzmann method provides a competitive numerical technique for solving many problems in computational fluid dynamics utilizing parallel machines.

ACKNOWLEDGMENTS

We thank H. Chen, K. Diemer, D. Grunau, Y. C. Lee, L. Luo, D. O. Martinez, W. H. Matthaeus, and David Montgomery for helpful discussions. This work is supported by the U.S. Department of Energy at Los Alamos National Laboratory, by DOE DE-FG02-85ER-53194, and by the NASA Innovative Research Program under grant NAGW 1648 and NASA NAG-W-710. Numerical simulations were done on the CM-2 at the

Advanced Computing Laboratory at Los Alamos National Laboratory. Some of the computations were supported by the NSF San Diego Supercomputing Center.

REFERENCES

1. U. Frisch, B. Hasslacher, and Y. Pomeau, *Phys. Rev. Lett.* **56**:1505 (1986).
2. G. McNamara and G. Zanetti, *Phys. Rev. Lett.* **61**:2332 (1988).
3. F. Higuera, S. Succi, and R. Benzi, *Europhys. Lett.* **9**:345 (1989).
4. D. H. Rothman and J. M. Keller, *J. Stat. Phys.* **52**:1119 (1988).
5. J. A. Somers and P. C. Rem, *Physica D* **47**:39 (1991).
6. S. Chen, G. D. Doolen, K. Eggert, D. Grunau, and E. Y. Loh, *Phys. Rev. A* **43**:245 (1991).
7. D. H. Rothman, *Geophysics* **53**(4): 509 (1988).
8. S. Chen, K. Diemer, G. D. Doolen, K. Eggert, C. Fu, and B. Travis, *Physica D* **47**:72 (1991).
9. H. Chen and W. H. Matthaeus, *Phys. Rev. Lett.* **58**:1845 (1987).
10. S. Chen, H. Chen, D. Martinez, and W. H. Matthaeus, *Phys. Rev. Lett.* **67**:3776 (1991).
11. H. Chen, S. Chen, and W. H. Matthaeus, *Phys. Rev. A* **45**:R5339 (1992).
12. S. Succi, R. Benzi, and F. Higuera, *Physica D* **47**:219 (1991).
13. U. Frisch, D. d'Humiéres, B. Hasslacher, P. Lallemand, Y. Pomeau, and J.-P. Rivet, *Complex Systems* **1**:649–707 (1987).
14. S. Wolfram, *J. Stat. Phys.* **45**:19–74 (1986).
15. E. Y. Loh, private communication.
16. S. Chen, G. D. Doolen, D. Grunau, S. Gutman, and S. Lustig, Modeling non-Newtonian fluids with a lattice Boltzmann equation method, preprint (1991).
17. S. A. Orszag, *Lecture Notes in Computer Science*, Vol. 11, G. Goos, Karlsruhe, and J. Hartmanis, eds. (Springer-Verlag, 1974).
18. R. H. Morf, S. A. Orszag, and U. Frisch, *Phys. Rev. Lett.* **44**:572 (1980).
19. M. Brachet, D. I. Meiron, S. A. Orszag, B. G. Nickel, R. Morf, and U. Frisch, *J. Fluid Mech.* **130**:411 (1983).
20. H. Chen, J. R. Herring, R. M. Kerr, and R. H. Kraichnan, *Phys. Fluids* **1**(11):1844 (1989).
21. S. Chen, Z. Wang, G. D. Doolen, and X. Shan, Lattice Boltzmann simulations for three dimensional turbulent flows, in preparation (1991).
22. A. Vincent and M. Meneguzzi, *J. Fluid Mech.* **225**:1891 (1991).
23. Zhensu She, private communication.